Cent. Eur. For. J. 71 (2025) 207–223 sciendo DOI: 10.2478/forj-2025-0007

CENTRAL EUROPEAN Forestry Journal

ORIGINAL PAPER

Efficient and cost-effective monitoring of urban green spaces using combination of photogrammetry, LiDAR, and RTK in an iPhone-Based approach

Jozef Výbošťok[1], Juliána Chudá[1], Michal Skladan[1], Arunima Singh[2], Daniel Tomčík[1], Martin Mokroš[3]*

[1]*Technical University in Zvolen, Department of Forest Harvesting, Logistics and Ameliorations, T. G. Masaryka 24, SK-960 01 Zvolen, Slovakia*

[2]*Q-ForestLab, Department of Environment, Ghent University, Ghent, Belgium*

[3]*University College London, Department of Geography, North-West Wing, Gower Street, UK-WC1E 6BT London, United Kingdom*

Abstract

Urban green spaces (UGS) provide various ecological, cultural, aesthetic, and psychological functions contributing to public health and well-being. To ensure proper management and the optimal performance of all these functions, it is essential to closely monitor their structure: number of trees, species composition, tree size, health status, location and surrounding objects. Traditionally, parameters are measured using conventional methods: calipers, altimeters, and diameter tapes. However, while modern 3D data collection technologies such as terrestrial and mobile laser scanners or photogrammetry have been employed for monitoring UGS, their use is often challenging. Therefore, we aimed to test and create a methodology using a novel device (Pix4D & Emlid Scanning Kit), which uniquely combines photogrammetry and light detection and ranging with real-time kinematics in a smartphone. Since the solution is smartphone-based, it provides relatively low-cost employability. The research was conducted in Adolf Priesol Park in Zvolen (Slovakia) over an area of approximately 6,000 m^2. We focused on the device's positional accuracy in measuring footpaths, park amenities, and trees, as well as its tree detection rate and accuracy in determining tree diameter. The results demonstrated that the device exhibited high positional accuracy (horizontal RMSE = 0.08 m, vertical RMSE = 0.07 m), a 100% tree detection rate, and exceptional diameter at the breast height accuracy, with an RMSE of 1.1 cm in the area-based approach and 0.42 cm in the individual approach. Notably, the 6,000 m^2 area was covered in 80 minutes, including collecting almost 85 trees, all footpaths and all park amenities.

Key words: urban green space; Emlid; photogrammetry; LiDAR

Editor: Bohdan Konôpka

1. Introduction

Urban green spaces (UGS) are considered an essential element in the design of the urban landscape (Li et al. 2021) which perform several functions such as ecological, cultural, aesthetic, and psychological functions, contributing to public health and well-being (Grêt-Regamey et al. 2013). They are also important in regulating microclimate (Richardson & Isebrands 2013; Li et al. 2018; Tang et al. 2023) and air purifying (Hirabayashi 2021). They provide many services to citizens, providing space for sports activities, relaxation, and mitigation to tackle heat (Wang & Wu 2020; Wang et al. 2023).

Mapping and monitoring of UGS by collecting data on the structure, such as the number of trees, species composition, tree size, health status, and location, are essential for estimating indicators like total leaf area and tree biomass. These metrics are crucial for quantifying various forest functions and ecosystem services, which are important for effective urban forest planning and enhancing the quality of life in cities (Nowak et al. 2008; Shekhar & Aryal 2019). Given the lack of comprehensive information about vegetation in urban environments, UGS mapping should be a fundamental step in sustainable urban planning (Shekhar & Aryal 2019).

In both the past and present, various methods have been employed to collect data for UGS mapping and

Corresponding author. Martin Mokroš, e-mail: m.mokros@ucl.ac.uk

monitoring. These methods include field measurements using tools such as diameter tape, caliper, and hypsometer, as well as the interpretation of aerial and satellite images (Holopainen et al. 2013). While field measurements can provide accurate UGS information, they are often time-consuming, expensive, and usually unable to cover large areas (Cabo et al. 2018; Chen et al. 2019; Shahtahmassebi et al. 2021). Aerial and satellite imagery, on the other hand, offer the advantage of acquiring data over large areas but are limited in their ability to capture sufficient detail due to relatively low spatial resolution (Pu & Landry 2012; Shahtahmassebi et al. 2021). We cannot overlook the fact that modern non-contact data collection methods, such as airborne laser scanning (ALS) and unmanned aerial vehicle scanning (ULS), are increasingly being used to monitor UGS (Zięba-Kulawik et al. 2021; Schmohl et al. 2022). ALS provides data at lower point densities, is widely used in urban areas, and allows efficient mapping over larger areas, with minimal constraints from flight regulation. ULS, on the other hand, delivers very high point density and detail, which is advantageous when analysing individual trees and structures in detail. However, this technology faces limitations in urban areas due to strict regulations on aerial activities that may affect its use (Bruggisser et al. 2019). Due to these limitations, it is necessary to explore and develop innovative ground-based solutions that can be effectively used in specific applications, for this let us return to the ground solution.

A suitable alternative to these methods could be the utilization of close-range remote sensing methods capable of generating 3D point clouds, such as terrestrial photogrammetry and laser scanning. These methods are currently gaining more and more popularity and attention. Laser scanning utilizes light detection and ranging (LiDAR) to measure distances between a scanner and an object of interest to create 3D representations as a point cloud (Roberts et al. 2019). Based on mobility, Laser scanning can be divided into static laser scanning, also known as terrestrial laser scanning (TLS), where the objects are scanned from a static position on a tripod, and mobile laser scanning (MLS), where scanning is performed while the scanner is in motion (Liang et al. 2016; Hyyppä et al. 2020). TLS generates a point cloud of the highest quality with a high level of spatial accuracy, on the other hand, TLS is expensive and requires significant labour and time. Due to its static nature, objects of interest must be scanned from multiple positions to mitigate occlusion effects, particularly in complex terrain. Additionally, the high accuracy and detail of TLS generate a large amount of data, requiring powerful computing resources and substantial storage capacity. TLS is particularly suited for detailed measurement of small areas with high detail and point density. It is widely used in architecture, construction, archaeology, automation systems, etc. (Holopainen et al. 2013). TLS has also found its applications in forestry and forest inventories (Liang et al. 2018; Ritter et al. 2020), estimation of dendrometric parameters such as diameter at breast height (DBH), tree height, and stand volume (Astrup et al. 2014; Cabo et al. 2018; Zięba-Kulawik et al. 2021). It is also used for mapping and monitoring urban greenery (Jaalama et al. 2021; Zięba-Kulawik et al. 2021). The drawbacks of TLS, such as occlusion, time consumption, and laboriousness, can be mitigated using MLS (Černava et al. 2019; Mokroš et al. 2021).

MLS devices can be handheld, mounted on a backpack, or attached to a vehicle (such as a quad bike or tractor). In these cases, scanning is performed while the scanner is in motion, ensuring the object is captured from multiple perspectives. These devices typically use SLAM (Simultaneous Localization and Mapping) technology to link individual scans (Bauwens et al. 2016; Balenović et al. 2021). SLAM determines the location and orientation of a device in the local coordinate system at a specific moment in time using the detected objects while simultaneously creating a map of the surroundings (Bauwens et al. 2016; Balenović et al. 2021; Mokroš et al. 2021). From a user point of view, the MLS is easier to use. The drawback compared to TLS is lower spatial accuracy and lower point density, point clouds contain more noise, which can lead to false tree detection and duplications, especially in denser stands (Mokroš et al. 2021), MLS has a wide range of applications in various areas. There are many publications about MLS utilization in forest environments and it finds utilization in area of UGS.

MLS and TLS technologies are relatively expensive, and an affordable alternative to them could be terrestrial photogrammetry, which has recently flourished. With the development of computer technology and the SfM (structure from the motion) algorithm, by using 2D images with sufficient overlap, it is possible to create 3D point clouds that are approaching the accuracy of point clouds from laser scanning (Tomaštík et al. 2017; Mokroš et al. 2018; Liang et al. 2022). The main advantage of terrestrial photogrammetry is its affordability (Roberts et al. 2019): however, creating a usable 3D point cloud is largely dependent on the camera settings, environmental conditions, and the scanning pattern chosen by the operator and, more importantly, it is time-consuming and requires operator's expertise (Piermattei et al. 2019). All these limitations can make this method difficult and prone to failure, making it less usable than laser scanning (Roberts et al. 2019). Terrestrial photogrammetry has the potential to be used in the measurement of various dendrometric parameters also finds its application in the mapping of urban green areas.

Recently, a new technology was introduced to the market named RTK-Pix4D & Emlid scanning kit. This kit creates lidar-photogrammetric point clouds in an automated way by combining three technique: RTK (Real-Time Kinematic) for precise positioning, photogrammetry for aligning collected images, and LiDAR sensor in a mobile phone (https://docs.emlid.com/reachrx/integration/pix4dcatch/).

This device offers a promising method for photogrammetric point cloud creation and can minimize the drawbacks of traditional SfM photogrammetry. To the authors' knowledge, no studies have yet been published evaluating this technology.

The aim of this paper is to assess the potential of this technology for monitoring urban green spaces. The novelty of this study lies in the 3D data collection and analysis with a revolutionary, low-cost, and user-friendly device combining LiDAR, photogrammetry, and RTK, where the basic element is a smartphone with a LiDAR sensor.

The study aimed to identify the potential of the application of this new technology in monitoring UGS. Specifically, we aimed to answer the following questions:

– What positional accuracy can be achieved with this device when measuring UGS components (trees, footpaths, and park amenities)?
– What is the tree detection rate and the accuracy of determining the DBH of trees?
– What is the time and cost-effectiveness of monitoring UGS with this device?

2. Methodology

2.1. Study site

The study was conducted in the urban park of Prof. Adolf Priesol in Zvolen, central Slovakia (48.572904°, 19.118490°). As public spaces, the urban park comprises impervious surfaces, grassed areas, and mixed plantings of tree species. The vegetation coverage of the park exceeded 80%. The main vegetation types are deciduous broadleaved trees, evergreen broadleaved trees, and shrubs. Five subplots (A, B, C, D, and E) were established in the park, with A, B, and C being smaller in size compared to D and E. The surfaces of the park trails are mainly asphalt. The number of trees varied from 4 to 43 across the five subplots (all trees considered), with DBH varying from 4.8 to 110.1 centimetres. There are 8 trees in subplot A, 10 trees in subplot B, 4 trees in subplot C, 43 trees in subplot D, and 20 trees in subplot E (Fig. 1) – 85 trees in total.

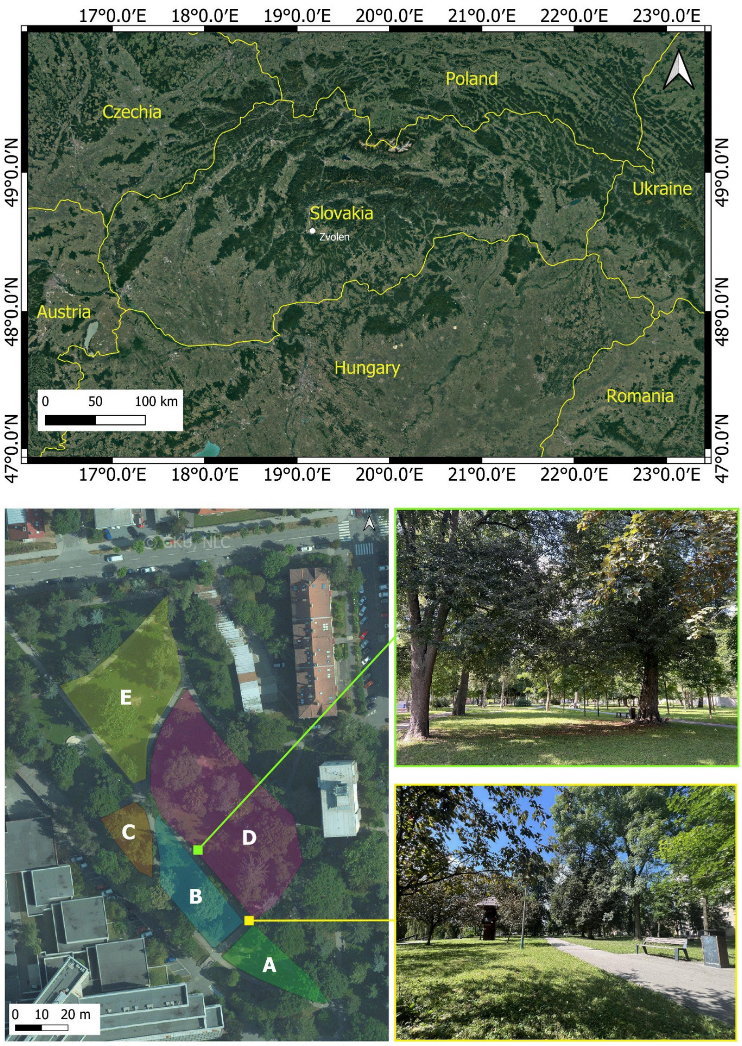

Fig. 1. Up: Overview map showing the location of the town of Zvolen. Bottom Left: Situation map showing the location of subplots A, B, C, D, and E within the study site. Bottom Right: Photographs of the study site in the urban park of Prof. Adolf Priesol in Zvolen.

2.2. RTK-Pix4D & Emlid scanning kit

Description of Devices and Software

The mobile laser scanning solution with RTK – Pix4D & Emlid Scanning kit was used for the data collection. The device combines the Emlid Reach RX Multi-band ultralight RTK rover and Pix4D Scanning kit solution for making 3D scans. An Apple iPhone 15 Pro Max controlled the mapping device. The PIX4Dcatch mobile app was used to control the device. The Emlid Scanning Kit, when used with Pix4D software, combines photogrammetry and LiDAR capabilities using the iPhone. Photogrammetry involves capturing multiple images from different angles to create 3D models (Fig. 2).

The Emlid Reach RX device enhances the accuracy of these images by providing precise geotagging, which is crucial for creating accurate 3D reconstructions. The LiDAR sensor on the iPhone provides real-time feedback during image capture. It helps fine-tune the positioning and pose information, ensuring the images are accurately triggered. During processing, LiDAR data is used to estimate a more accurate scale of the reconstruction and to fill low-texture areas that photogrammetry alone might not be able to reconstruct (emlid.com).

When using the Pix4D & Emlid Scanning Kit, the iPhone connects via Bluetooth to the Emlid Reach RX GNSS receiver. Then, PIX4Dcatch mobile app for iOS devices was used. App allows users to acquire detailed and georeferenced data for 3D models using photogrammetry and LiDAR technology simultaneously (PIX4Dcatch). In the PIX4Dcatch app, you can then choose whether you want to acquire the location using the sensors integrated in the iPhone or via an external antenna, such as the Emlid Reach RX (Integration of Reach RX for iPhones with LiDAR).

Further PIX4Dmatic desktop software was used. These tools work together so that data captured by PIX4Dcatch is imported and processed in PIX4Dmatic for post-processing and advanced analysis for 3D model creation (PIX4Dcatch datasets in PIX4Dmatic). The software is designed to process large datasets from photogrammetry and LiDAR, allowing fast and accurate processing of thousands of images with precision suitable for Surveying (PIX4Dmatic). The software uses the accurate data obtained from photogrammetry to align LiDAR images, minimizing biases caused by drift of GPS and inertial measurement unit (IMU) sensors in mobile devices.

A key challenge addressed by device is the problem of GNSS and IMU drift on mobile devices. This occurs due to the real-time position and orientation estimation (PIX4Dmatic 1.19: combined LiDAR and photogrammetry workflow | Pix4D).

In the context, iPhone'integrated ARKit plays a significant role in enhancing data accuracy during 3D scanning. ARKit is an augmented reality framework developed by Apple that allows to create interactive AR on iOS devices. Considering device position, ARKit uses the device's sensors, such as the accelerometer, gyroscope, and compass, to track the device's motion and orientation in real time. This data enables the accurate positioning of virtual objects in the real world and their interaction with the real environment (ARKit – Augmented Reality). The data collected by ARKit is combined with camera data, including location and time of collection, contribut-

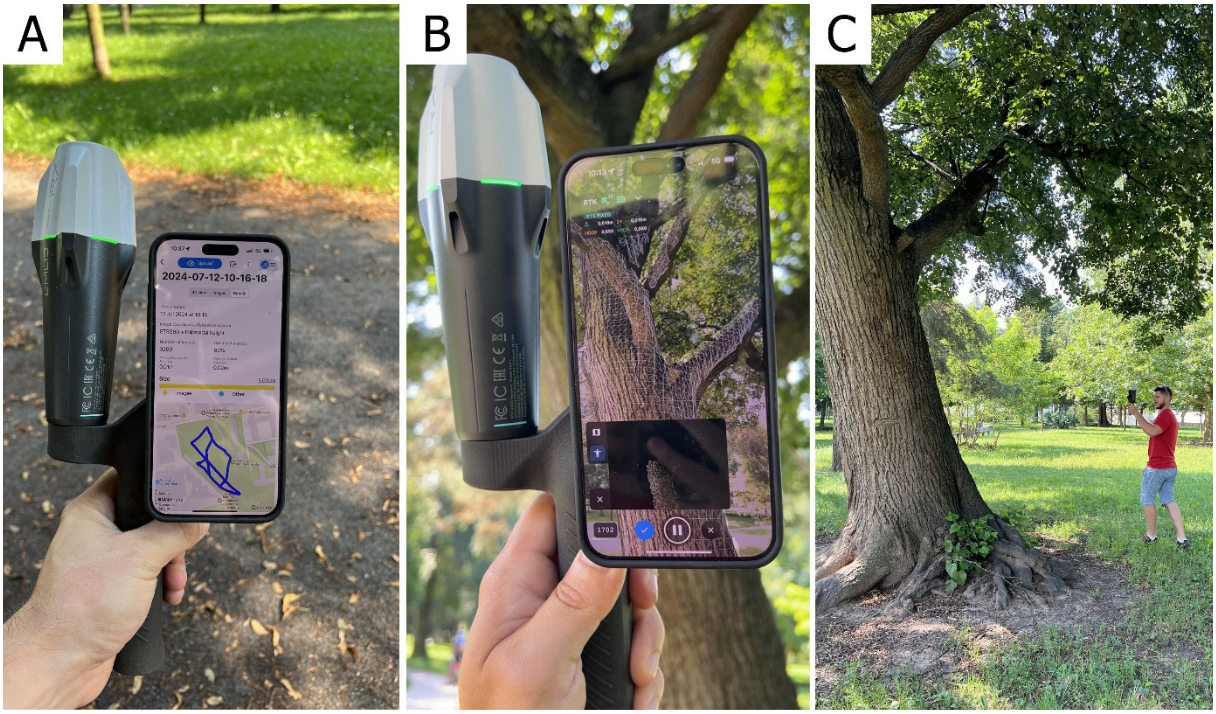

Fig. 2. Pix4D & Emlid Scanning kit in field. A: footpath scanning, B: tree scanning IA, C: tree scanning ABA.

ing to a more accurate location of virtual objects in the real world. In applications PIX4Dcatch, ARKit works with an external GNSS receiver the Emlid Reach RX to provide more accurate position and orientation data. Here, users can choose whether they want to use position data from ARKit or from an external device, depending on accuracy requirements and the environment.When capturing data with devices equipped with LiDAR scanners, ARKit provides real-time position and orientation estimations (Pix4DEmlidScanningKit). However, these estimations can sometimes drift, leading to misalignment in LiDAR scans and potential inaccuracies (Explore ARKit). As a result, LiDAR scans taken by the device can become misaligned, leading to inaccurate data. PIX4Dmatic resolves this issue by calculating more precise geolocation and orientation data during photogrammetric processing. This accurate information is then used to properly align the LiDAR scans, ensuring that the LiDAR data is also accurate (PIX4Dmatic 1.19: combined LiDAR and photogrammetry workflow | Pix4D).

Data Collection Methodology

We used the default settings in the app: 90% image overlap, and under the 'Image Trigger Method' section, Distance (device pose) set to 10 cm and Angle set to 20 degrees. This mean a picture is automatically take only if distance from the previous photoshoot changes by 10 cm and the device rotates by 20°. Each subplot was scanned in a single session, ensuring all trees within the subplot were recorded sequentially without revisiting the same site multiple times. Additionally, the operator only started the motion when the device reported satisfactory signal quality (FIX) for high-accuracy positioning.

The experiment focuses on the device's usability for prompt mapping of urban areas and consists of several phases (Fig. 3). In the first phase, measurements of the footpaths were taken in the park, with the utmost care being taken to avoid multiple passes over a single location during the scanning process. This concluded the first experimental "footpath" layer. More emphasis was done on creating a quality record for reference points located on the footpaths. The second part of the experiment involved creating a 3D point cloud of the park amenities (benches, trash cans, memorials). The objects were captured in the "benches and bins" layer. The objects in the research area were walked around in a uniform rectilinear motion to record them from every angle, thus creating a plausible image of the objects and allowing visual identification of the reference points located on them. In the third part of the experiment, we focused on the accuracy of the device for DBH and tree positions estimation using 2 approaches – the Individual approach (IA) and the Area-based approach (ABA). For IA a selection of 30 trees of varying ages and species was made, and each tree was individually scanned to create a separate point cloud. For the IA approach, each tree was both scanned and processed separately as a separate project. In the ABA approach, we scanned individual subplots sequentially to ensure that all trees within a subplot were recorded at the desired quality. Footpaths, park amenities, and ABA subplots were scanned and processed as separate projects.

During the scanning, the operator constantly checked the quality of GNSS solution the status RTK Fixed is most required. In case of a failure, for example due to movement under the tree canopy which forms a physical barrier to the GNSS antenna, the operator stopped for a few seconds and waited for the FIX solution. However, in not all cases this solution was achieved, in which case the data collection continued along the planned trajectory and the FIX solution was achieved at another data collection trajectory point when conditions improved.

2.3. Reference data collection

When creating the methodology for testing the positional accuracy of the new device, we considered the basic assumption that the highest positional accuracy will be achieved at permanently stabilized points in optimal conditions and by measuring with standard geodetic methods – points on the pavement stabilized with geodetic nails. For this experiment, reference data were collected in the form of coordinates for 36 points located on the park footpath stabilized with geodetic nails and marked with orange spray (for "footpath" layer evaluation). Subsequently, we drove into the dataset 24 points located on

Fig. 3. Point cloud visualization – details. A: wooden monument detail, B: foothpath reference point detail, C: woodbark detail, D: bins and bench detail.

benches and trash cans marked with a permanent marker ("benches and bins" layer), objects that have straight and defined edges, on which it is relatively easy to measure or estimate the position of a specific point but there is already a higher potential for error. And lastly coordinates and DBH of 85 trees across the study site ("tree" layer). For objects such as trees in general, there can be an error from extrapolation because we are considering a point inside the trunk, on its axis and the cross-section of the tree trunk is not circular but ellipsoidal.

The reference data was acquired in one day Emlid scanning kit and also the Global Navigation Satellite System (GNSS). Geodetic survey was performed using a Topcon 9000 total station in combination with GNSS antenna Topcon Hiper SR. The real-time kinematic (RTK) method was used to measure the standpoints of the total station, and the positions of reference points and tree positions in the research plots were subsequently measured. Standpoints for the total station were positioned to optimize conditions for RTK use, ensuring the highest possible accuracy within 1 cm. To determine the position of each tree, a point on the trunk was first measured at a mark 1.3 meters above the ground (the DBH measurement position), and the angle and distance from the total station were recorded. Later, during office work, the trunk radius for each tree was added to the distance from the total station, and the orthogonal coordinates for the trees were calculated.

The perimeters of trees were measured by measuring tape. Before the measurement, the trees were numbered with biodegradable, easily erasable paint, and the DBH measurement point was marked on each trunk so that the mark was visible in the resulting point cloud Fig. 4A.

2.4. Post-processing of data

Post-processing of data from the Pix4D & Emlid scanning kit was performed in PIX4Dmatic (PIX4D SA. (2024). PIX4Dmatic (Version 1.63.0) [Computer software]. https://www.pix4d.com). For ABA, subplots A to E were scanned and processed one after the other. For IA each tree was scanned and processed separately. The workflow included calibration with predefined parameters (Pipeline – Trusted location and orientation, Image scale 1/1 – original image scale, Key points – auto, Low internal confidence), where the images are used to perform key point extraction, key point matching and camera optimization, followed by re-optimization where internal and external camera parameters were updated, image pre-processing, and generation of a point cloud with hight density.

A total of 11,931 pictures were collected, and out of these 11,890 pictures were calibrated in an ABA of tree scanning and in scanning the footpaths 3,299 pictures were collected and all of them were calibrated and for park amenities consistently, just as many photos were calibrated as were taken – 1,688. For the IA, 3,078 pictures were collected, and 3,077 pictures were subsequently calibrated (Table 1).

Table 1. Summary of the number of pictures entering the dense point cloud production process in the PIX4Dmatic 1.63.0

	Subplot	Number of images	Number of calibrated images
Tree ABA	A	755	754
	B	1,510	1,510
	C	640	640
	D	6,086	6,064
	E	2,940	2,922
	Total	11,931	11,890
Footpath		3,299	3,299
Park amenities		1,688	1,688
Tree IA		3,078	3,077

According to our previous experiences with SfM photogrammetry, during the processing of the projects and the creation of the final point cloud, the system performed reliably without any issues, which is not always the case when processing photogrammetric images (Fig. 5).

After processing in PIX4Dmatic, all clouds were in real coordinate system due to the use of GNSS antenna in data acquisition.

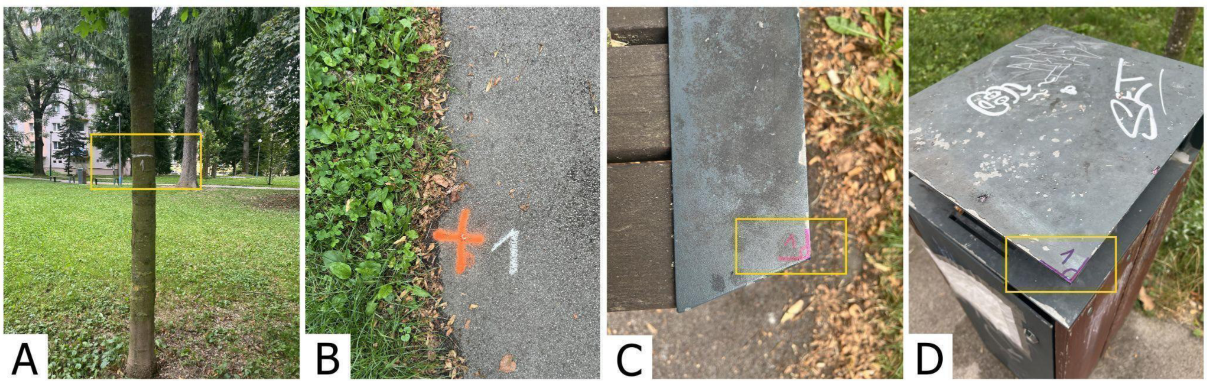

Fig. 4. Reference data collection – points stabilization visualization. A: DBH and tree position measurement point, B: footpath point, C: bench point, D: trashcan point.

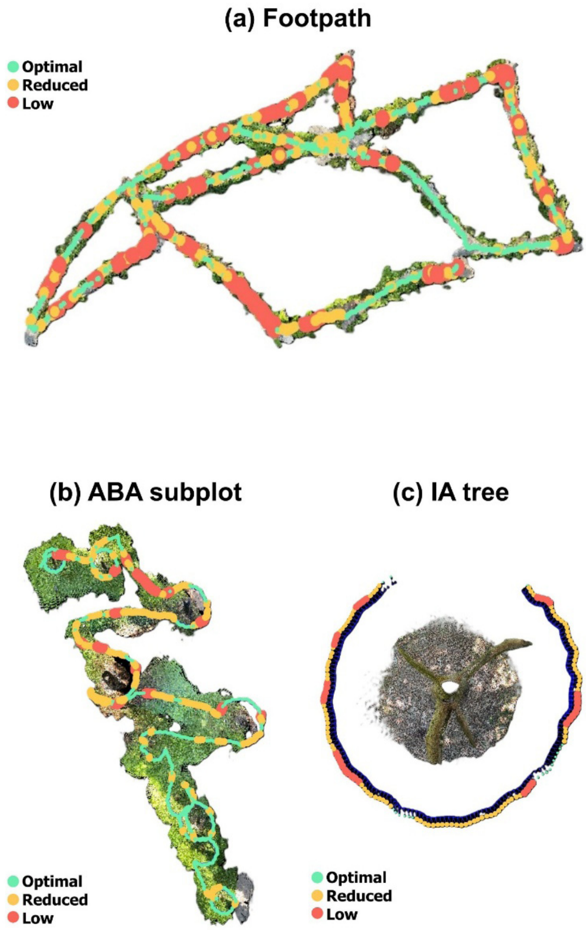

Fig. 5. Visualization of the GNSS solutions in connection with generated point clouds: (a) Footpath point cloud, (b) ABA subplot point cloud, (c) IA single tree point cloud. GNSS Solution: Green – Optimal (RTKFixed – the highest accuracy), Orange – Reduced solution, Red – Low quality solution.

Point clouds were processed in CloudCompare (CloudCompare (version 2.12) [GPL software]. (2021). Retrieved from http://www.cloudcompare.org.) where object positions were manually extracted to evaluate position accuracy. To estimate DBH, 2 cm thick cross-sections were created in CloudCompare directly at the marker on the trunk. The cross-section was exported in .txt format and thus attached for further processing (DBH estimation from perimeter in QGIS). Also, the coordinates of geodetic nails, bench, and trash points were manually extracted for the "footpath" and "benches and bins" layer. In the point cloud, a specific nail on the foothpath/point on the bench was manually identified and a estimated coordinate was identified using the Point picking tool. Fig. 6 visualizes the exported dense point clouds focusing on detail for each data collection approach.

2.5. DBH Estimation and Tree detection rate

Tree detection rate (TDR) was determined by manual identification based on the position of trees in the subplots:

$$TDR = \frac{n_{found}}{n_{ref}} \cdot 100 \qquad [1]$$

where n_{found} represents number of identified trees and n_{ref} is number of all considered trees (30 for IA and 85 for ABA).

Each tree was manually identified by its position, and then a 2 cm thick cross-section was manually created from the point cloud at the corresponding mark on the trunk, as mentioned in the previous part of the text. The CloudCompare was used for this purpose. To evaluate the

Fig. 6. Point cloud visualization.

accuracy of tree position and DBH, the point cloud cross-sections were created at the mark placed directly at the point of the DBH measurement in the field. These cross-sections were then processed in QGIS 3.16.3, where the tree perimeter was manually measured and converted to DBH (Fig. 7). To obtain the estimated DBH, a polygon accurately describing the outer perimeter was manually created for each cross section, the length of which was recalculated to diameter in the next step.

2.6. Statistical analysis

The error of the estimated positions was expressed as the difference between the reference and the estimated position, separately for each axis (X, Y and Z):

$$e_{i(x)} = x_{ref} - x_{est} \qquad e_{i(y)} = y_{ref} - y_{est} \qquad e_{i(z)} = z_{ref} - z_{est} \qquad [2]$$

where, *ref* represents value measured via conventional methods and *est* means estimated value.

The discrepancies between these coordinates were quantified using the Root Mean Square Error (RMSE), which provides an average measure of the coordinate error. RMSE values were calculated for each direction, offering a comprehensive assessment of the accuracy of the outputs relative to the reference data.

Calculation of the root mean square direction errors:

$$RMSE_H = \sqrt{\frac{\sum_{i=1}^{n} (\Delta x_i^2 + \Delta y_i^2)}{n}} \quad RMSE_V = \sqrt{\frac{\sum_{i=1}^{n} \Delta z_i^2}{n}} \quad [3]$$

where, Δx_i, Δy_i, and Δz_i represents the differences between the reference coordinates and the coordinates estimated from the estimated data, where n denotes the total number of points in the dataset.

A Hotelling's T^2 test was applied to evaluate the mean differences between estimated and reference coordinates. Hotelling's T^2 test is a multivariate extension of the Student's t-test, designed to assess whether the mean vector of a multivariate dataset significantly deviates from a specified reference point. In this study, the test was applied to evaluate systematic deviations in the estimated object positions compared to reference measurements. Specifically, the test examined whether the mean differences in the x, y, and z coordinates between the estimated and reference positions were statistically different from zero, indicating positional bias. The test was performed separately for each object. This analysis was performed using the R software (R Core Team 2024).

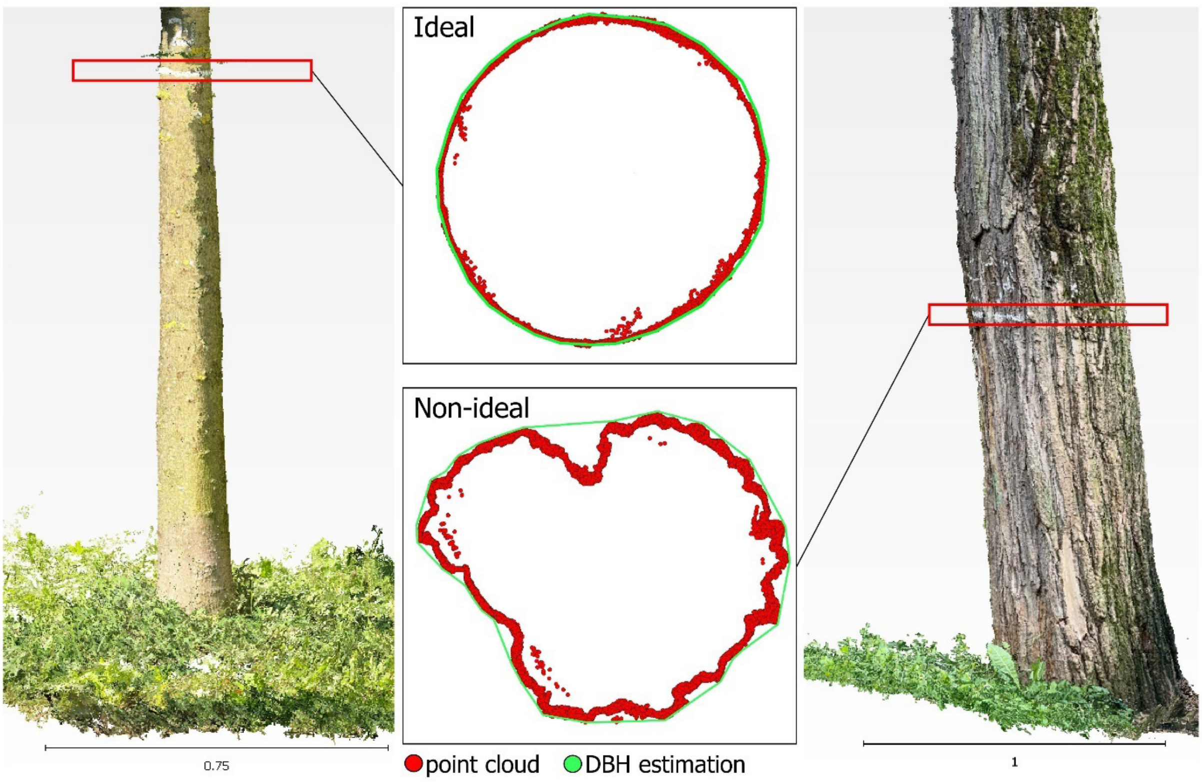

Fig. 7. Example of DBH estimation from 3D point clouds on two cross-sections with varying shapes: an ideal circular shape (top) and a non-ideal irregular shape (bottom). The red points represent the point cloud, while the green line indicates the DBH estimation.

3. Results

3.1. Positional accuracy

The spatial accuracy was evaluated on 175 validation points across four distinct object types: 24 park amenities points located on benches and bins, 36 footpath points, 30 tree positions acquired by IA, and 85 tree positions acquired by ABA.

The first experiment aimed to compare the positions of the points from point clouds collected using a Pix4D & Emlid scanning kit device to the measurement conducted using a precise surveying point included in the "benches and bins" layer. The distribution of positional errors for various objects is illustrated using the boxplot shown in Fig. 8. The boxplot analysis for the error reveals several key insights into the accuracy and variability of the coordinates across different objects. The median errors for most objects and coordinates are close to zero, indicating a general lack of systematic bias in the spatial estimated values. The Interquartile Range (IQR), representing the middle 50% of the data, varies across objects. Notably, the trees-ABA exhibits a higher IQR, particularly in the vertical direction, indicating greater variability in the vertical positioning of trees. In contrast, objects like "footpaths" and "benches and bins" show lower IQR values, suggesting more consistent estimated values.

Appendices Fig. A1 and Fig. A2 present the RMSEs and the results of t-tests assessing whether the errors differ significantly from zero, by direction and object.

Root mean square error (RMSE) of coordinates for various objects are shown in Fig. 9. The highest vertical error was obtained for the IA (0.116 m). Conversely, the smallest vertical error was achieved in the footpath layer evaluation (0.039 m). The highest error in the horizontal direction is observed for the ABA to tree position detection (0.082), followed by the error associated value for the IA evaluation (0.065). The smallest error in the horizontal direction was again obtained when evaluating the points on the footpath (0.026). The RMSE analysis reveals that the highest errors occur in the horizontal direction for trees–ABA and in the vertical direction for trees–IA.

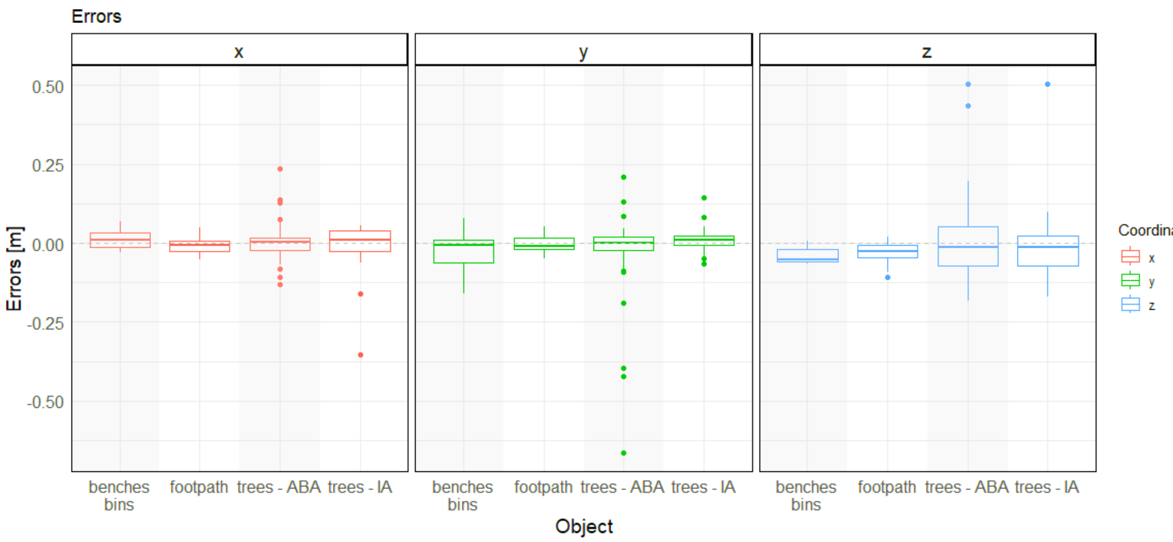

Fig. 8. Positional error of x, y, and z direction grouped by object.

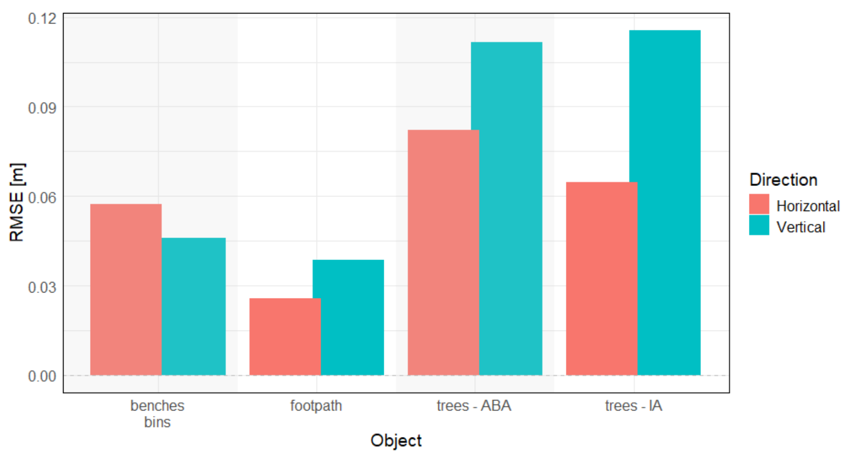

Fig. 9. Bar plot of RMSE values grouped by objects (x-axis) and direction (color).

The Hotelling's T^2 test revealed statistically significant differences in the estimated and reference positions for "benches and bins" and "footpath", indicating systematic positional bias in these objects (Table 2). These results suggest that the estimated positions for "footpath" and "benches and bins" exhibit significant deviations across the x, y, and z coordinates, reflecting potential systematic errors in their spatial measurements. In contrast, no statistically significant differences were observed for "trees-ABA" and "trees-IA", indicating that the estimated positions for these tree-related objects are consistent with the reference values. These findings indicate that while objects such as "footpath" and "benches and bins" exhibit systematic positional deviations, the ABA and IA tree approaches do not present a statistically significant difference in their positional accuracy. Thus, positional errors in tree datasets are likely within acceptable measurement tolerances. A higher T^2 value (Table 2) indicates a greater deviation between the estimated and reference positions across multiple dimensions (x, y, z).

Table 2. Results of the Hotelling's T^2 test for statistical differences in Estimated and Reference measurements. Statistically significant differences are reported as *** for $p < 0.001$.

Object	T^2 Value	p-value
benches and bins	9.952	< 0.001***
footpath	26.172	< 0.001***
trees-ABA	1.57	0.287
trees-IA	1.28	0.22

3.2. DBH Estimation and TDR

The TDR for the ABA on all subplots is 100%, it was even possible to detect all the shrubs in the subplots. The results of the linear regression, (Fig. 10) confirmed a strong relationship between reference and estimated DBH for both ABA ($r^2 = 0.988$) and IA ($r^2 = 0.999$). Overall, a smaller error was achieved with the IA RMSE = 0.462 compared to the ABA, where the RMSE reached 1.051.

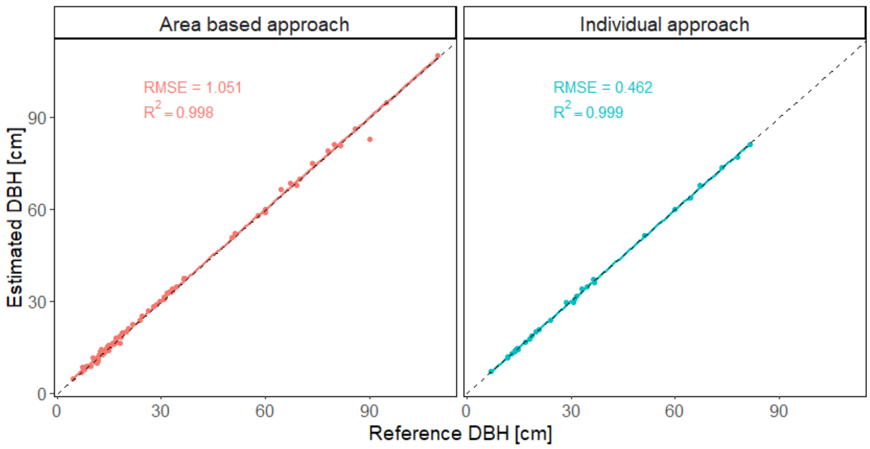

Fig. 10. Linear regression of estimated dbhs according to ABA (left) and IA (right).

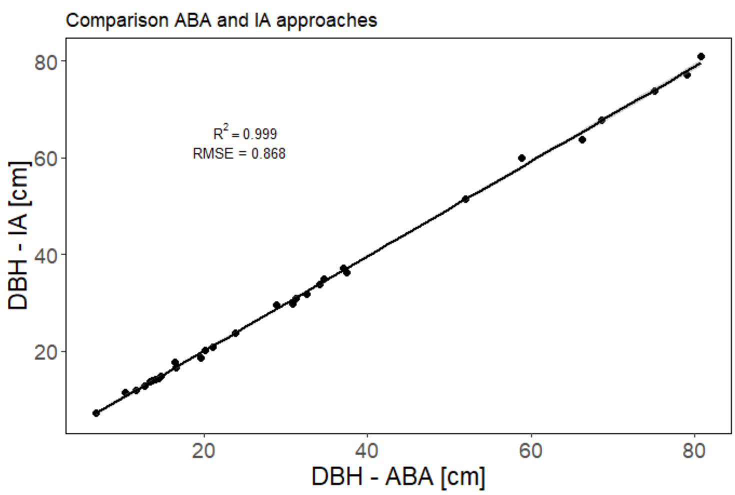

Fig. 11. Linear regression of estimated DBHs for 30 selection trees from IA and their corresponding values obtained from ABA.

An evaluation of the impact of the method on the accuracy of DBH determination was performed on 30 pairs of derived DBHs of identical trees from IA and ABA (Fig. 11).

The correlation results show a strong dependence between the DBH estimated from ABA and IA. A paired t-test was performed for pairs of estimated DBHs ($t = 1.3655$, $df = 29$, p-value = 0.1826). There is no statistically significant difference between the ABA and IA DBHs based on paired T-test, as the p-value is 0.1826, which is greater than the typical 0.05 significance level. This is also suggested by the similar RMSE values: it is 0.868 for ABA(30 trees) and 0.426 for IA.

3.3. Effectivness

Data collection was completed in 1 hour and 20 minutes using the tested device (Table 3). In contrast, the traditional method using a diameter tape and total station required 3 hours and 38 minutes, more than twice the time. Overall, the total time required for data acquisition and processing, from initial data collection to the generation of the complete 3D point cloud, was 70 hours and 26 minutes.

4. Discussion

This study showed the potential application of mobile terrestrial scanning solution with RTK-Pix4D & Emlid Scanning Kit. The experiment was conducted in several phases, such as positional accuracy assessment, DBH estimation, TDR, and evaluation of the method's effectiveness.

Each subplot was scanned in one session, making sure all trees in the subplot were recorded in order without revisiting the same site. The general finding is that when the same object is scanned multiple times, the quality of the point cloud depends on the quality of the GNSS signal. If the solution was FIX – high positional accuracy – the point density increased correctly. However, if the positioning accuracy decreased, duplication of points and noise around the object were created.

The spatial accuracy was evaluated on 175 validation points across four distinct object types to compare the positions of the points from point clouds collected using a Pix4D & Emlid scanning kit device to the measurement conducted using precise surveying equipment (Topcon 9000 total station). Positional error was calculated as the difference between the reference and estimated position, with horizontal (x, y) and vertical (z) directions analyzed separately (Fig. 9). We used RMSE for each direction (horizontal and vertical), which provided a comprehensive assessment of the accuracy of the outputs compared to the reference data. The highest horizontal error was found for the ABA tree positions (0.082 m), while the highest horizontal accuracy was achieved at points on the footpath. The geodetic nails at the footpath were in good conditions in terms of GNSS signal, and because the points were small, the operator concentrated on making sure they were picked up during collection – slowing down slightly over each point. This meant that the recording took slightly longer in these good conditions. The RTKfix was more straightforward to achieve on the footpath because of the more open canopy layer. The highest vertical error was found for the IA method (0.116 m), while the lowest error was observed for the foothpath points again (0.039 m).

The RMSE analysis of tree position showed the highest errors in the horizontal direction for ABA and in the vertical direction for IA trees (Fig. 9). We consider signal degradation at positions with limited view of satellites to be the main source of errors.We assume that the higher horizontal error in ABA may be due to a slight deformation of the strains in the point cloud caused by the different signal quality during the data collection, but since the

Table 3. Time-consumption table.

Plot	Calibration[a]	Depth point cloud[b]	Dense point cloud[c]	Depth & dense fusion[d]	Data collection[e]	Data acquisition[f]	Total
A	1:57:48	0:01:46	1:47:13	0:02:55	0:06:00	0:14:00	4:09:42
B	4:49:25	0:06:30	5:03:00	0:11:05	0:07:00	0:18:00	10:35:00
C	0:18:18	0:02:08	1:03:26	0:04:03	0:03:00	0:07:00	1:37:55
D	16:04:47	0:38:32	13:22:01	3:07:58	0:23:00	1:17:00	34:53:18
E	7:25:45	0:07:39	6:59:01	0:16:52	0:13:00	0:36:00	15:38:17
footpath	0:23:04	0:07:37	1:14:53	0:12:52	0:18:00	0:12:36	2:29:02
equipment	0:12:16	0:03:52	0:19:28	0:03:45	0:10:00	0:14:00	1:03:21
Total	31:11:23	1:08:04	29:49:02	3:59:30	1:20:00	2:58:00	70:25:59

Note:
[a] Calibration is the first step in processing. The images and additional inputs, such as GCPs are used to perform keypoints extraction and matching, camera model optimization-and geolocation.*
[b] Depth point cloud is generated from iPhone's LiDAR.*
[c] Dense point cloud is generated from images using photogrammetry.*
[d] Depth & dense fusion combines the dense point cloud with the depth point cloud allowing a better point cloud.*
[e] Data collection – in field.
[f] Data acquisition – validation point coordinate/DBH estimation.

*source: https://support.pix4d.com/hc/pix4dmatic error is around 2 cm, we consider the result to be friendly. The use of a total station to determine the trunk center is also found in other studies, but the authors often do not provide details on the calculation methods (Qian et al. 2017; Fan et al. 2018).To determine the reference trunk axis position, it was necessary to adjust the tree position to the center of the trunks, which can be problematic for trees with irregular shapes. We used a similar procedure in our previous work, where we adjusted each tree by 1/2 of its DBH in the direction of measurement (The method records the horizontal angle and distance of the object from the total station's position and orientation point - the direction with a zero horizontal angle. During office work, the distance to each tree is adjusted by 1/2 DBH to accurately place the point at the tree's center (Chudá et al. 2024), which we consider to be an accurate approach. We do not reject this approach as a source of potential error, but we consider it insignificant.

Although objects such as benches or baskets were expected to produce very accurate results, the Hotelling's T^2 test (Table 2) revealed statistically significant differences in the estimated and reference positions for "benches and bins" and "footpath" layers, although these objects were expected to have accurate positioning due to their regular shape and good GNSS availability. Thus, the systematic error of "benches and bins" and "footpath" is evident from the T^2 test (Table 2), with a p-value < 0.001 indicating that there are outliers that are significant enough to be considered systemic. Numbers such as 9.952 and 26.172 indicate stronger variations in the positions of these objects, which may be due to various factors such as sensor accuracy or environmental influences. For tABA and IAtree positions these biases were not significant, suggesting that for these objects the methods are more stable and less prone to bias.The systematic errors for "benches and bins" may be due to various influences such as inaccuracies in the definition of reference points, noise in the data, or environmental factors (e.g., interference from GNSS signals). In contrast, for trees, these influences are likely to have been compensated for by adjustments to the position of the centre of the trunk, resulting in lower variability and smaller system errors.The results of other authors showed more biases in the vertical position compared to the horizontal (Hartzell et al. 2018; Wujanz et al. 2018; Brown et al. 2020). One of these publications proposed a method to evaluate the accuracy of airborne LiDAR data by using a TLS, which helps avoid the influence of point density, rather than relying on single GNSS points. The relative and absolute accuracies were tested for iPhone 13 pro using Modelar's scanning application and found that the absolute accuracy varies ±3 cm horizontally and ±7 cm vertically (Chase et al. 2022). Therefore, the positional accuracy of the device (Pix 4D) achieved is sufficient for park monitoring.

The TDR was found to be 100%. With the combined use of GNSS, LiDAR, and photogrammetry, it was possible to create a point cloud of a thin tree. For thin trees, it was possible to reconstruct the trunk up to a height of 1.7 m with this 3D data acquisition method, 4.2 m for medium trees, and 5.8 m for the thickest trees. The range is, of course, also influenced by the branching of the trunk. There are two major advantages over classic photogrammetry. Firstly, the possibility of checking the real-time view of the reconstructed point cloud. Secondly, the detection of shrubs using the photogrammetry method. With the tested device, detecting and creating high-quality shrub models was possible. It was considered a success because, with classical photogrammetry, capturing and subsequently modeling such complex structures, like bushes, is often challenging (Torkan et al. 2023).

Data collection using the device under test took 1 hour and 20 minutes (Table 3), whereas the traditional method, which involved measuring the DBH a diameter tape and using a total station, took 3 hours and 38 minutes, more than twice as long. The total time required for data collection and processing, from initial data collection to generation of the complete 3D point cloud, was 70 hours and 26 minutes. Although the number appears high, it should be noted that the processes ran automatically without user involvement, meaning that this time can be invested in other tasks.This result shows not only cost-effectiveness, but also a significant improvement in process efficiency compared to traditional methods.

A comparative analysis of the low-cost mobile mapping systems (TLS, MLS, personal laser scanning (PLShh) – iPad Pro, and multicamera prototype) was conducted to evaluate the tree detection rate. The results showed that the iPad Pro's performance was close to TLS when DBH > 7 cm was considered (Mokroš et al. 2021). Following that, the comparison of MLSs, was also addressed in our previous research where MLSs and their effectiveness were tested for measuring DBH in fast-growing trees plantation (Skladan et al. 2025). In terms of equipment and operating costs, e.g., the MLS scanner Stonex X120GO MLS which is capable of collecting the cloud-point coloration in a real coordinate system, including the necessary data processing software, is in the range of approximately 30,000 to 35,000 EUR. The iPhone 15 Pro Max, which is priced between EUR 850 and EUR 1,200, represents a more affordable alternative. However, a GNSS antenna needs to be attached to the iPhone, which costs around EUR 2 000. However, additional software is also needed to generate 3D point clouds from photos. In this study, we used Agisoft Metashape Professional software, with an academic license costing approximately EUR 800 and a commercial license costing up to EUR 3,200 (prices are based on the supplier's official offers). But on the other hand, although the prices of total stations vary (starting at a few thousand and going up), it is important to consider the time savings in field measurements and the possibility to obtain comprehensive data in a shorter time, which can be significant advantages when using research equipment.

After the detection of the tree, DBH was estimated using two different approaches, namely ABA and IA. The correlation R^2 value found for both the approaches is very similar; however, the RMSE value observed for the ABA is higher than the IA, which represents more bias in the estimation of DBH with the ABA. There was no statistically significant difference between IA and ABA in position or thickness; however, ABA was more time-efficient. In the case of individual tree monitoring, better quality, and accuracy of the point cloud, the IA approach is more reliable. The DBH was also estimated using an individual tree scanning approach, and an R^2 value of 0.973 was found compared to TLS, which was 0.996. This also showed that the multi-scan mode in iPad Pro creates more ambiguities in the tree scanning due to the rescanning of the same tree as compared to the single tree scan mode (Mokroš et al. 2021; Wang et al. 2021).

The total time and effort required for data collection and pre-processing were higher compared to traditional methods, mainly due to the reconstruction of tree trunks and the ability to track changes over time. This feature is exclusive to this technology and is crucial for monitoring urban green spaces (UGS). The highest error was observed in the tree datasets, while the lowest error was recorded for the park footpaths. No statistical significance was found, but even with the largest errors, the results were still acceptable for monitoring the position of objects in the park.The effectiveness of the method was also evaluated by analyzing the time taken by the device to complete the processing. The method proved effective across all subplots, including the footpath and equipment, although the efficiency varied between them. Subplot D showed higher effectiveness, likely due to the larger number of images (6,086) involved.

Comparing our results with studies by other authors, we can conclude that the speed of data collection using MLS – PLShh (LiDAR iPhone included) varies significantly depending on the technologies used, with traditional methods such as diameter tape and total station measurements still requiring significantly more time. The data collection rate for other methods, such as the PLShh, is comparable or even faster. Our results show high efficiency in data collection, other studies, such as Skladan et al. (2025), also show that other PLShh technologies can be very fast for data collection and processing, with low time requirements. This suggests that new PLShh technologies may be suitable for fast and efficient processing in the field, but with lower cost-effectiveness. In Skladan et al. (2025), data collection for a single 30 × 30 m study area took less than 5 minutes using PLShh Stonex X120GO (approximately 55 min per ha), while processing the raw data using GOpost software took approximately 20 minutes, but the price of the device is almost EUR 35 000. Using an iPhone or iPad to measure DBH and positions of all trees in the research plot in the 25 × 25 m forest plot in Mokros et al. (2021) took 15 minutes with the iPad LiDAR (approximately 4 h per ha) and 10 minutes with the iPhone 13 Pro Max LiDAR (approximately 2 h 30 min per ha). Using an iPhone and iPad to measure DBH and positions of all trees in a 1 ha area took 1 hour 39 minutes (iPhone) and 1 hour 38 minutes (iPad), while using the traditional method with a tape measure and total station took 3 hours 13 minutes for two people (Tatsumi et al. 2023). In all cases, the data collection is aimed at obtaining a point cloud of the entire area, whereas Tatsumi uses Forest-Scanner, which only needs to point the phone briefly at a tree and estimate DBH.

Our data processing time (70 hours and 26 minutes) may seem high, but this figure includes a complex process from collection to the generation of the 3D point cloud. Comparison with other approaches such as Mokroš et al. (2021), who report approximately 10h:35m:00s as the total collection and processing time for the iPad scan of 25 × 25 research plot, shows that the LiDAR system on the iPhone may be faster in the initial collection, but processing may still take longer depending on the size and complexity of the dataset.

Although the system achieves high accuracy, the sensor range of LiDAR-enabled iPhones is limited to 5 meters, limiting the ability to effectively capture objects at greater distances. This limit may be particularly important when collecting data for large areas or in complex forest and park environments where wider areas need to be covered. In such cases, it may be necessary to use other technologies or approaches mentioned above. In the context of the previous discussion, the range of the LiDAR sensor in the device is a key limiting factor that affects the quality of the acquired data, especially when measuring trees and objects in more challenging environments. However, for certain tasks and specific scenarios where the short range of the LiDAR is sufficient for accurate data collection, this limit may be acceptable, especially when the added value is the saving of time, money and human labor, which has proven to be an advantage in our results. Therefore, even if the range of the LiDAR sensor presents a limit, the system provides sufficiently high quality outputs and, in some cases, completely replaces the need for more costly devices.

This research highlights the potential of the Pix4D & Emlid scanning kit to accurately map trees in urban environments, which aligns with previous studies on tree mapping accuracy. Moreover, this method is also capable of producing highly precise models of shrubs, which is less common in traditional photogrammetry methods. However, if the device described by us should be used in practice, then, for larger areas, it is necessary to divide area of interest into smaller sub-areas due to the limitations of the smartphone's memory and RAM.

In accordance with recent studies (Gollob et. al 2021; Mokroš et al. 2021; Wang et al. 2021; Tatsumi et al. 2023; Oikawa et. al 2025), our results demonstrate that this low-cost mobile mapping approach can be a viable alternative to more conventional techniques for both trees and shrubs, offering new opportunities for urban green space monitoring.

5. Conclusion

We presented the potential of using low-cost equipment to create 3D point clouds in challenging environments. The conditions found in urban parks closely resemble those in real forests (dense vegetation, variable canopy cover, complex terrain), as both face similar GNSS-related issues. This study demonstrates that a low-cost iPhone-based mapping approach – integrating photogrammetry, LiDAR, and RTK – can provide highly accurate and detailed three-dimensional (3D) data for monitoring UGS. Moreover, these findings are relevant for forest stands with higher tree densities, where similar GNSS challenges and device limitations can occur. As we continue testing in more complex environments, we anticipate that the results will further confirm the viability of this approach in forests and high-density urban parks, while also identifying potential limitations, especially when working with smaller DBH trees or more obstructed environments.The assessment of 175 validation points covering footpaths, benches and bins, and tree positions confirmed sub-decimetre RMSE in all coordinate directions, with the highest spatial accuracy observed in partially open environments such as footpaths. Even under partial canopy cover, tree positions were accurately reconstructed, highlighting the device's reliability in less-than-ideal GNSS conditions. This result demonstrated that the system achieves high positional accuracy, providing sufficiently accurate outputs in certain tasks, thereby eliminating the need for a total station.This not only eliminates the necessity for total station measurements but also provides added value through enhanced efficiency. DBH estimates from both scanning approaches – the area-based and individual, correlated strongly with reference measurements ($R^2 > 0.98$). Although the ABA introduced slightly higher errors in DBH (RMSE = 1.05 cm) than the IA (RMSE = 0.46 cm), there was no statistically significant difference between these two approaches for the same trees. This confirms that the new technology can satisfy the requirements of comprehensive UGS assessments – whether for large-scale mapping or individual tree-level inventories.The time and cost benefits are also considerable. In this study, scanning 6,000 m^2, capturing more than 85 trees, footpaths, and park amenities, took only 80 minutes in the field. While post-processing remains more time-consuming than traditional surveying, the value gained – such as detailed 3D models and robust metrics for UGS management – outweighs the added computational effort. In comparison with conventional survey methods, which are time consuming and lack the detail in comparison with point clouds, the presented approach offers a efficient workflow suitable for periodic, high-resolution monitoring UGS. Further, the main disadvantage is the range of the smartphone's lidar which makes it impossible to reconstruct whole trees, in our case the models for thick trees had a height of 5.8 m so it is not possible to measure the heights of the trees, but for quick measurement of the positions of trees, footpaths or park amenities as well as the derivation of the DBH, the device is suitable, highly efficient and economically advantageous due to the low purchase price compared to handheld scanners. The device can also be used in the forest, but its performance will be limited primarily by the quality and availability of the GNSS signal, which will be a critical factor in achieving accurate results. Overall, this research underlines the potential of a lates low-cost LiDAR-and-photogrammetry method enhanced by RTK for urban forestry applications.

Acknowledgements

The paper was supported by the Slovak Research and Development Agency APVV-20-0391 "Monitoring of forest stands in three-dimensional space and time by innovative close-range approaches", and by the Ministry of Education of Slovak Republic grant project VEGA 1/0604/24 "Development of a prototype mobile scanning system for monitoring the condition and evolution of forest ecosystems", Funded by the EU NextGenerationEU through the Recovery and Resilience Plan for Slovakia under the project No.09I03-03-V04-00341 and No. 09I03-03-V05-00016.

References

Astrup, R., Ducey, M. J., Granhus, A., Ritter, T., von Lüpke, N., 2014: Approaches for estimating stand-level volume using terrestrial laser scanning in a single-scan mode. Canadian Journal of Forest Research, 44:666–676.

Balenović, I., Liang, X., Jurjević, L., Hyyppä, J., Seletković, A., Kukko, A., 2021: Hand-held personal laser scanning–current status and perspectives for forest inventory application. Croatian Journal of Forest Engineering, 42:165–183.

Bauwens, S., Bartholomeus, H., Calders, K., Lejeune, P., 2016: Forest inventory with terrestrial LiDAR: A comparison of static and hand-held mobile laser scanning. Forests, 7:127.

Brown, R., Hartzell, P., Glennie, C., 2020: Evaluation of SPL100 Single Photon Lidar Data. Remote Sensing, 12:722.

Bruggisser, M., Hollaus, M., Kükenbrink, D., Pfeifer, N., 2019: Comparison of forest structure metrics derived from UAV LiDAR and ALS DATA. ISPRS Annals of the Photogrammetry, Remote Sensing and Spatial Information Sciences, IV-2/W5:325–332.

Cabo, C., Del Pozo, S., Rodríguez-Gonzálvez, P., Ordóñez, C., González-Aguilera, D., 2018: Comparing terrestrial laser scanning (TLS) and wearable laser scanning (WLS) for individual tree modeling at plot level. Remote Sensing, 10:540.

Černava, J., Mokroš, M., Tuček, J., Antal, M., Slatkovská, Z., 2019: Processing chain for estimation of tree diameter from GNSS-IMU-based mobile laser scanning data. Remote Sensing, 11:615.

Fan, Y., Feng, Z., Mannan, A., Khan, T. U., Shen, C., Saeed, S., 2018: Estimating Tree Position, Diameter at Breast Height, and Tree Height in Real-Time Using a Mobile Phone with RGB-D SLAM. Remote Sensing, 10:1845.

Grêt-Regamey, A., Celio, E., Klein, T. M., Wissen Hayek, U., 2013: Understanding ecosystem services tradeoffs with interactive procedural modeling for sustainable urban planning. Landscape and Urban Planning, 109:107–116.

Gollob, C., Ritter, T., Kraßnitzer, R., Tockner, A., Nothdurft, A., 2021: Measurement of Forest Inventory Parameters with Apple iPad Pro and Integrated LiDAR Technology. Remote Sensing, 13:3129.

Hirabayashi, S., 2021: Technical specifications of urban forests for air purification: A case study in Tokyo, Japan. Trees, Forests and People, 4:100078.

Holopainen, M., Kankare, V., Vastaranta, M., Liang, X., Lin, Y., Vaaja, M. et al., 2013: Tree mapping using airborne, terrestrial and mobile laser scanning: A case study in a heterogeneous urban forest. Urban Forestry & Urban Greening, 12:546–553.

Hyyppä, E., Kukko, A., Kaijaluoto, R., White, J. C., Wulder, M. A., Pyorala, J. et al., 2020: Accurate derivation of stem curve and volume using backpack mobile laser scanning. ISPRS Journal of Photogrammetry and Remote Sensing, 161:246–262.

Hyyppä, E., Yu, X., Kaartinen, H., Hakala, T., Kukko, A., Vastaranta, M. et al., 2020: Comparison of backpack, handheld, under-canopy UAV, and above-canopy UAV laser scanning for field reference data collection in boreal forests. Remote Sensing, 12:203327.

Chase, P. P. C., Clarke, K. H., Hawkes, A. J., Jabari, S., Jakus, J. S., 2022: Apple IPhone 13 Pro LiDAR Accuracy Assessment for Engineering Applications. Conference of Transforming Construction with Reality Capture Technologies: The Digital Reality of Tomorrow, Fredericton, New Brunswick, Canada, p. 1–10.

Chen, S., Liu, H., Feng, Z., Shen, C., Chen, P., 2019: Applicability of personal laser scanning in forestry inventory. PLoS ONE, 14:22.

Chudá, J., Výbošťok, J., Tomaštík, J., Chudý, F., Tunák, D., Skladan, M. et al., 2024: Prompt Mapping Tree Positions with Handheld Mobile Scanners Based on SLAM Technology. Land, 13:93.

Jaalama, K., Kauhanen, H., Keitaanniemi, A., Rantanen, T., Virtanen, J.-P., Julin, A. t al., 2021: 3D Point Cloud Data in Conveying Information for Local Green Factor Assessment. ISPRS International Journal of Geo-Information, 10:762.

Li, T., Zheng, X., Wu, J., Zhang, Y., Fu, X., Deng, H., 2021: Spatial relationship between green view index and normalized differential vegetation index within the Sixth Ring Road of Beijing. Urban Forestry & Urban Greening, 62:127153.

Li, X., Ratti, C., Seiferling, I., 2018: Quantifying the shade provision of street trees in urban landscape: A case study in Boston, USA, using Google Street View. Landscape and Urban Planning, 169:81–91.

Liang, X., Kankare, V., Hyyppä, J., Wang, Y., Kukko, A., Haggrén, H. et al., 2016: Terrestrial laser scanning in forest inventories. ISPRS Journal of Photogrammetry and Remote Sensing, 115:63–77.

Liang, X., Hyyppä, J., Kaartinen, H., Lehtomäki, M., Pyörälä, J., Pfeifer, N. et al., 2018: International Benchmarking of Terrestrial Laser Scanning Approaches for Forest Inventories. ISPRS Journal of Photogrammetry and Remote Sensing, 144:137–179.

Liang, X., Kukko, A., Balenovic, I., Ninni, S., Junttila, S., Kankare, V. et al., 2022: Close-Range Remote Sensing of Forests: The State of the Art, Challenges, and Opportunities for Systems and Data Acquisitions. IEEE Geoscience and Remote Sensing Magazine, 2–41.

Mokroš, M., Liang, X., Surový, P., Valent, P., Černava, J., Chudý, F. et al., 2018: Evaluation of Close-Range Photogrammetry Image Collection Methods for Estimating Tree Diameters. ISPRS International Journal of Geo-Information, 7:93.

Mokroš, M., Mikita, T., Singh, A., Tomaštík, J., Chudá, J., Wężyk, P. et al., 2021: Novel low-cost mobile mapping systems for forest inventories as terrestrial laser scanning alternatives. International Journal of Applied Earth Observation and Geoinformation, 104.

Nowak, D. J., Crane, D. E., Stevens, J. C., Hoehn, R. E., Walton, J. T., Bond, J., 2008: A Ground-Based Method of Assessing Urban Forest Structure and Ecosystem Services. Arboriculture & Urban Forestry, 34:347–358.

Hartzell, P., Dang, Z., Pan, Z., Glennie, C., 2018: Radiometric Evaluation of an Airborne Single Photon Lidar Sensor. IEEE Geoscience and Remote Sensing Letters, 15:1466–1470.

Oikawa, N., Nakagawa, Y., Owari, T., Tatsumi, S., Suzuki, S. N., 2025: Utilising LiDAR-equipped iPhone in forestry: Constructing 3D models and measuring tree sizes in a planting site. Ecological Solutions and Evidence, 6:e12399.

Piermattei, L., Karel, W., Wang, D., Wieser, M., Mokroš, M., Surový, P. et al., 2019: Terrestrial structure from motion photogrammetry for deriving forest inventory data. Remote Sensing, 11:950.

Pu, R., Landry, S., 2012: A comparative analysis of high spatial resolution IKONOS and WorldView-2 imagery for mapping urban tree species. Remote Sensing of Environment, 124:516–533.

Qian, C., Liu, H., Tang, J., Chen, Y., Kaartinen, H., Kukko, A. et al., 2017: An integrated GNSS/INS/LiDAR-SLAM positioning method for highly accurate forest stem mapping. Remote Sensing, 9:1–16.

Richardson, J., Isebrands, J. G., 2013: Poplars and Willows: Trees for Society and the Environment. Proceedings of the 13th North American Agroforestry Conference, June 19–21, 2013, Charlottetown, Prince Edward Island, Canada, p. 35–37.

Ritter, T., Gollob, C., Nothdurft, A., 2020: Towards an Optimization of Sample Plot Size and Scanner Position Layout for Terrestrial Laser Scanning in Multi-Scan Mode. Forests, 11:1099.

Roberts, J., Koeser, A., Abd-Elrahman, A., Wilkinson, B., Hansen, G., Landry, S. et al., 2019: Mobile Terrestrial Photogrammetry for Street Tree Mapping and Measurements. Forests, 10:701.

Schmohl, S., Narváez Vallejo, A., Soergel, U., 2022: Individual Tree Detection in Urban ALS Point Clouds with 3D Convolutional Networks. Remote Sensing, 14:1317.

Shahtahmassebi, A. R., Li, C., Fan, Y., Wu, Y., Gan, M., Wang, K. et al., 2021: Remote sensing of urban green spaces: A review. Urban Forestry & Urban Greening, 57:126946.

Shekhar, S., Aryal, J., 2019: Role of geospatial technology in understanding urban green space of Kalaburagi city for sustainable planning. Urban Forestry & Urban Greening, 46:126450.

Skladan, M., Chudá, J., Singh, A., Masný, M., Lieskovský, M., Pástor, M. et al., 2025: Choosing the right close-range technology for measuring DBH in fast-growing trees plantations. Trees, Forests and People, 19:100747.

Tang, L., He, J., Peng, W., Huang, H., Chen, C., Yu, C., 2023: Assessing the visibility of urban greenery using MLS LiDAR data. Landscape and Urban Planning, 232:104662.

Tatsumi, S., Yamaguchi, K., Furuya, N., 2023. ForestScanner: A mobile application for measuring and mapping trees with LiDAR-equipped iPhone and iPad. Methods in Ecology and Evolution, 14:1603–1609.

Tomaštík, J., Mokroš, M., Saloň, Š., Chudý, F., Tunák, D., 2017: Accuracy of Photogrammetric UAV-Based Point Clouds under Conditions of Partially-Open Forest Canopy. Forests, 8:151.

Torkan, M., Janiszewski, M., Uotinen, L., Rinne, M., 2023: Method to Obtain 3D Point Clouds of Tunnels Using Smartphone LiDAR and Comparison to Photogrammetry. IOP Conference Series: Earth and Environmental Science, 1124:012016.

Wang, X., Singh, A., Pervysheva, Y., Lamatungga, K. E., Murtinová, V., Mukarram, M. et al., 2021: Evaluation of iPad Pro 2020 LiDAR for estimating tree diameters in urban forest. ISPRS Annals of the Photogrammetry, Remote Sensing and Spatial Information Sciences, VIII-4:105–110.

Wang, X., Wu, C., 2020: An Observational Study of Park Attributes and Physical Activity in Neighborhood Parks of Shanghai, China. International Journal of Environmental Research and Public Health, 17:2080.

Wang, X., Rahman, M. A., Mokroš, M., Rötzer, T., Pattnaik, N., Pang, Y. et al., 2023: The influence of vertical canopy structure on the cooling and humidifying urban microclimate during hot summer days. Landscape and Urban Planning, 238:104841.

Wujanz, D., Avian, M., Krueger, D., Neitzel, F., 2018: Identification of stable areas in unreferenced laser scans for automated geomorphometric monitoring. Earth Surface Dynamics, 6:303–317.

Zięba-Kulawik, K., Skoczylas, K., Wężyk, P., Teller, J., Mustafa, A., Omrani, H., 2021: Monitoring of urban forests using 3D spatial indices based on LiDAR point clouds and voxel approach. Urban Forestry & Urban Greening, 65:127324.

Other sources

R Core Team, 2024: R: A language and environment for statistical computing (version 4.3.2). R Foundation for Statistical Computing, Vienna, Austria. Available at https://www.R-project.org/.

Appendix

Fig. A1. Barplot of RMSE split by objects (x axis) and coordinates (colour).

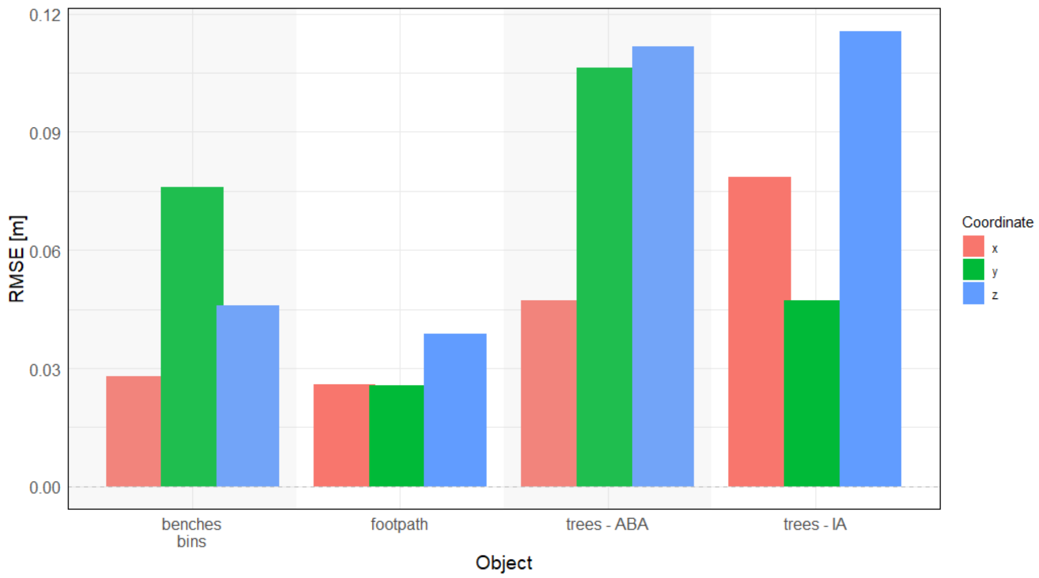

Fig. A2. Comparison of errors to zero using t-test. Statistically significant differences are reported as follows: *** for $p < 0.001$, ** for $p < 0.01$, * for $p < 0.05$.